State-dependent forces in cold quantum gases

Christopher Billington

Submitted in total fulfilment of the requirements
of the degree of Doctor of Philosophy

Supervisory committee:
Prof Kristian Helmerson
Dr Lincoln Turner
Dr Russell Anderson

School of Physics and Astronomy
Monash University

January, 2017

```
rev:     84 (cf53f98d7d0e)
author:  Chris Billington
date:    Wed Oct 11 18:15:11 2017 -0400
summary: Working on atomic physics spin stuff
```

This page intentionally left blank

Contents


```
rev:     84 (cf53f98d7d0e)
author:  Chris Billington
date:    Wed Oct 11 18:15:11 2017 -0400
summary: Working on atomic physics spin stuff
```

This page intentionally left blank

```
rev:     84 (cf53f98d7d0e)
author:  Chris Billington
date:    Wed Oct 11 18:15:11 2017 -0400
summary: Working on atomic physics spin stuff
```

Chapter I

Introduction

The subject of study of this thesis is Bose–Einstein condensation, as well as associated experimental and theoeretical techniques and phenomena in cold atom physics. The following chapters describe my work in a cold atom research group over the past several years, pertaining to apparatus construction, experiment, theory, and software design and development. An overarching theme is *state-dependent forces* on cold atoms. Selectively subjecting atoms to forces based on what state they are is at the core of many phenomena in cold atom physics. As I go into in the following chapters, different types of state selectivity allow for cooling and imaging techniques that would otherwise not be possible, momentum state-selectivity is central to wave-mixing phenomena; and semiclassical models run into a problem when state-selective forces cannot be disregarded in determining the classical force that atoms modelled semiclasically ought to be subjected to.

Bose–Einstein condensates (BECs) in dilute atomic gases are superfluids that can be created in the lab at extremely low temperatures. This strange state of matter was predicted in 1925 by Bose and Einstein [?, ?] , first produced experimentally in 1995 [?] in a cloud of rubidium atoms, and has since been made out of many other atoms, usually alkali metals [?, ?, ?, ?]. In a BEC, a macroscopic sample of bosonic atoms all occupy the same quantum state, and many of the features of the single particle wavefunctions are exhibited by the cloud as a whole. Bose–Einstein condensation and cold atoms more generally have rich applications in precision measurement [CITE], quantum computation [CITE] and quantum simulation.

1.1 Chapter overview

Various experimental techniques are used to produce and study Bose–Einstein condensates, many of which exploit of necessitate an understanding of the quantum behaviour of the atomic systems in question. I summarise some of these techniques and the atomic physics principles underlying them in chapter 2.

The fields of Bose–Einstein condensation and cold atoms more generally enjoy a tight coupling between theory and experiment, not least because of the enduring usefulness and accuracy of mean-field theory. In mean-field theory, the quantum matter field operator of the atoms comprising a Bose–Einstein condensate is replaced with its expectation value at each point in space, allowing the entire multi-particle system to be modelled with little more computational complexity than that required to model a single-particle wavefunction.[1] The resulting differential equation—the Gross–Pitaevskii equation—is nonlinear and using it to propagate a condensate wavefunction in time generally requires numerical techniques rather than analytic ones. My favourite numerical methods for

[1] mean field theory is accurate in the low-temperature limit, and even then is limited—it is unable for example to correctly model *s*-wave scattering of atoms when two BEC wavepackets are collided with each other [CITE], but it is good enough for comparison with a wide range of experiments regardless.

```
rev:     84 (cf53f98d7d0e)
author:  Chris Billington
date:    Wed Oct 11 18:15:11 2017 -0400
summary: Working on atomic physics spin stuff
```

doing so (which apply more generally to numerically evolving quantum systems of all kinds) are described in chapter **??**. In chapter **??** I also develop a variation on fourth-order Runge–Kutta integration which improves on one of its deficiencies for simulating quantum systems. I also present arguments that a fairly sophisticated method of discretising partial differential equations—the finite element discrete variable representation—may offer less computational efficiency that simpler methods for computing solutions of comparable accuracy to the Gross–Pitaevskii and Schrödinger wave equations.

As an experimental field, BEC research involves the construction of apparatuses capable of implementing the techniques described in chapter 2 in order to produce, control, and measure BECs. Chapter **??** describes some of the process of constructing such an apparatus, which involves a vacuum system, magnetic coils and optical systems. I present an optical layout for producing magneto-optically trapped ^{87}Rb atoms (a step on the way to condensation) that I designed and assembled as an exchange student in the group of József Fortágh at the University of Tübingen's Physikalisches Institut.

Production, control, and measurement of cold atom systems require more than the necessary optics and magnetic sources to be installed—they must be controllable in a time-accurate way in order to execute the necessary cooling processes, manipulate the system as desired, and observe the results. Production of a condensate takes on the order of tens of seconds, requiring precisely timed pulses of laser light at specific frequencies, sweeps of magnetic field strengths, and frequency sweeps of radio and microwave radiation. This cannot all be done by human experimenters alone, and so requires computer automation of some kind. In chapter **??** I reproduce our publication on a suite of software programs, the *labscript suite*. This software leverages modern software development techniques such as object orientation, abstraction and isolation as well as older principles—such as aspects of the Unix philosophy—to produce a powerful, maintainable, extensible system for designing, running and analysing shot-based experiments on commodity hardware.

As superfluids, BECs have zero viscosity and as such can support persistent flows. In classical fluid dynamics the absence of viscosity means that a fluid cannot support vorticity,[2] and must be irrotational. However, fluid circulation can still occur around points of zero fluid density, known as vortices. In BECs this circulation is also quantised, in units of h/m.

These quantised vortices are topological defects—the phase of the macroscopic wavefunction winds by a multiple of 2π around them, and is undefined at the center of the vortex core itself. Quantised vortices were observed in superfluid helium[3] in the early 1960s [**?**], and in BEC in a dilute atomic gas in 1999 [**?**]. The formation, dynamics and decay of these vortices are believed to be important for the study of superfluid turbulence [**?**].

In chapter **??** I present simulations exploring the feasibility of imaging these vortices in-situ using *tracer particles*. Atoms of one kind (^{87}Rb) may become trapped in the cores of quantised vortices in a condensate of another kind (^{41}K), and if imaged in a time-resolved way, reveal the motion of these vortices. A primary concern in any implementation of such a scheme is keeping the tracer atoms cold enough that they remain trapped in the vortex cores even as they scatter light for imaging. To that end, in chapter **??** I present modelling of a novel—if impractical—laser cooling scheme for Sisyphus cooling of ^{87}Rb atoms in a 34 G magnetic field— a field strength at which ^{87}Rb and ^{41}K repel each other strongly (leading to tighter trapping in the vortex cores).

In a BEC, the wavelike behaviour of matter is apparent, unlike at higher temperatures at which atoms are well described as classical particles. Not only are atoms in a BEC wavelike, they are described by a *nonlinear* wave equation. As with nonlinear optical systems, they therefore exhibit wave-mixing behaviour whereby a number of momentum states may interact to produce additional momentum states. In chapter **??** I describe our lab's four wave mixing experiment, which reproduced an existing result for BECs, and then our attempt at six wave mixing—a higher order effect (in the sense of perturbation

[2] This is because the motion of vorticity is described by a diffusion equation—with viscosity as the diffusion constant. When the diffusion constant is zero, there is no way for vorticity to enter the fluid from a boundary in the first place!

[3] In which 10% or so of the atoms undergo Bose–Einstein condensation.

```
rev:     84 (cf53f98d7d0e)
author:  Chris Billington
date:    Wed Oct 11 18:15:11 2017 -0400
summary: Working on atomic physics spin stuff
```

theory). We did not observe the expected six wave mixing, rather we saw *four* wave mixing despite the required resonance condition apparently being violated. This result agreed with mean-field theory simulations however, implying that the result was unlikely to be due to some experimental error.

Atoms have spin, and when other spin-projection states cannot be disregarded, mean-field theory for spinful BECs takes the form of multiple, interacting fields. This allows for richer nonlinear dynamics that a single-component BEC, with wave mixing producing new momentum states and new spin-projection states in tandem. In chapter **??** I present simulation results showing this "spin wave" mixing, although the main result is that—for ^{87}Rb at least—the effect is very small and unlikely to be experimentally observable in existing ^{87}Rb BEC experiments.

As mentioned above, at high temperatures (higher than that at which atoms Bose-condense) atoms are well described as classical particles. This is true in the sense that the wavelike nature of the atoms can be disregarded—they move through space like classical billiard balls obeying Newtonian mechanics. The internal state of the atoms, however—for example the state of an outer shell electron—may not be well modelled by classical mechanics. Even at room temperature, an electron is poorly described as a classical charged particle orbiting a nucleus. When there is *coupling* then, between this internal state of an atom and its motional state, the quantum-ness of the internal state can in some sense 'leak' into its motional state even if the motion is otherwise modelled well classically. The classic example of this is the Stern–Gerlach experiment [CITE], in which a beam of atoms splits into two beams as it passes through a magnetic field gradient. A similar situation arises for atoms in a magnetic trap—a common feature of cold atom experiments and often used in the final stage of cooling to BEC. To correctly model the losses of atoms from these traps, one needs to model the internal state of the atoms quantum-mechanically, but it is computationally expensive to also model their spatial motion using full quantum wavefunctions. We would like a way to model the atoms' motion classically, but in such a way that it can reproduce Stern–Gerlach separation—with modelled atoms taking one or the other trajectory probabilistically, with the probabilities consistent with those of a fully quantum treatment. In chapter **??** I present such a model, one that is based on a *hidden variable* carried around with each atom being modelled, which selects one of the atom's internal eigenstates. The apparent definiteness of the hidden variable allows the spatial motion part of the modelling to treat the atoms' spin projection degree of freedom as if it were in a definite state, allowing the modelling to take a single, definite trajectory. The hidden variable itself is evolved using a stochastic hidden variable theory that ensures its probability of corresponding to any particular spin-projection state is consistent with with the underlying quantum evolution of the atom's internal degrees of freedom.

rev: 84 (cf53f98d7d0e)
author: Chris Billington
date: Wed Oct 11 18:15:11 2017 -0400
summary: Working on atomic physics spin stuff

This page intentionally left blank

Chapter 2

Atomic physics: Experimental techniques and theory

- Descriptions of the relevant physics in atomic physics experiments: Doppler cooling and magneto-optical traps, Sisyphus cooling, dipole forces, Feshbach resonances, scattering theory, Bose–Einstein statistics. Show how the Hamiltonian of a 'two level' (32 levels, all things considered for ^{87}Rb D line) atom with fine structure, hyperfine structure and Zeeman splitting arises from consideration of the different angular momenta. Use this to derive the differential equations for the state populations of an atom in a driving laser field. Gross Pitaevskii equation for single species, dual species and spinor condensate.
- Doppler cooling
- Magneto-optical trapping
- Optical dipole trapping
- Two-body scattering and Feshbach resonances
- -> Include stuff from 3rd year report
- Spin, fine structure, and hyperfine structure
- Equations of motion for two level atom with hyperfine structure
- The Monte-Carlo wavefunction method
- Mean field theory for Bose–Einstein condensates
- -> Superfluid velocity
- -> Vortices

2.1 Cooling, trapping, and manipulating atoms

BECs provide such a tantalising opportunity for studying quantum phenomena not only because of their interesting properties, but also because of the level of control they afford. Many of the same techniques which allow experimentalists such control over their creation are also employed in the creation thereof, and many were discovered along the way to Bose–Einstein condensation.

```
rev:     84 (cf53f98d7d0e)
author:  Chris Billington
date:    Wed Oct 11 18:15:11 2017 -0400
summary: Working on atomic physics spin stuff
```

The main experimental techniques used to create BEC—and which we are and will be employing in that pursuit—are Doppler cooling, magneto-optical and dipole trapping, polarisation gradient (Sisyphus) cooling, and evaporative cooling.

These were discovered, perhaps by no coincidence, in roughly the same order as they are called for in a BEC experiment.

2.1.1 Doppler cooling

Doppler cooling, demonstrated in 1978 [?] is a consequence of the simple observation that atoms see the wavelength of incident light Doppler shifted depending on their velocity. This can be used to selectively transfer momentum to only fast-moving atoms, by tuning an incident laser slightly redder than would be required for a resonant absorption. If six lasers in counterpropagating pairs orthogonal to each other surround a cloud of atoms, the atoms can be cooled close to the *Doppler limit* [?, p 58]

$$k_B T_D = \frac{\hbar \Gamma}{2} \tag{2.1}$$

where Γ is the linewidth of the atomic transition. For the cooling transition used for Doppler cooling ^{87}Rb[1], this gives 146 μK, which is approximately a factor of a thousand too high for Bose-condensation. These atoms are also not trapped.

[1] The D_2 line, $5S_{\frac{1}{2}} \rightarrow 5P_{\frac{3}{2}}$, approximately 780 nm.

2.1.2 Magneto-optical and magnetic trapping

Magneto-optical trapping, first demonstrated in 1987 [?] comes from the realisation that a magnetic field can be used to *spatially* vary the detuning from resonance that the atoms in the above mentioned arrangement of lasers see. This is possible due to the Zeeman effect [?], in which the wavelengths of atomic transitions are shifted in a magnetic field.

If a field profile can be found which causes the transition to come closer to resonance as the atoms move away from a central point, then it forms a trap—atoms that stray too far from the center will absorb more strongly and be deflected back[2].

[2] The polarisations of the beams are such that absorption from the inward facing beam occurs, rather than from the one that would accelerate the atom further outward!

The field configuration used in an anti-Helmholtz one, with two coils opposite each other carrying opposing currents. The resulting magnetic field profile has a zero in the middle and increases in magnitude in all directions.

With the Doppler beams off, this magnetic field still provides a trapping potential, due to the magnetic dipole interaction:

$$V(\boldsymbol{r}) = -\boldsymbol{\mu} \cdot \boldsymbol{B}, \tag{2.2}$$

where $\boldsymbol{\mu}$ is the atomic magnetic moment, and $\boldsymbol{B}$ the magnetic field. This only traps some atomic spin states, and has losses due to spin-flips [?] near the field zero.

2.1.3 Optical trapping

Optical dipole trapping on the other hand relies on the *dipole force*, in which off-resonant light shifts the energy of the eigenstates of the combined atom-light system, the so called *dressed states*. This energy shift, called the *light shift*, depends on the intensity of the light, and so results in a potential that spatially varies as the intensity of the light. In the limit of large detuning (compared to Rabi frequency), this shift is given by [?, p 8]:

$$\Delta E = \frac{\hbar \Omega^2}{4\delta} \tag{2.3}$$

where δ is the detuning from resonance and the Rabi frequency is:

$$\Omega = \frac{eE_0}{\hbar} \langle 1|\boldsymbol{x}|2\rangle, \tag{2.4}$$

```
rev:     84 (cf53f98d7d0e)
author:  Chris Billington
date:    Wed Oct 11 18:15:11 2017 -0400
summary: Working on atomic physics spin stuff
```

where E_0 is the amplitude of the light's electric field and $\langle 1|\boldsymbol{x}|2\rangle$ is the dipole moment between the two states in a two-level system.

With the potential proportional to E_0^2, and thus the light's intensity, the force the atom experiences is proportional to the light's intensity gradient. For this reason, the dipole force is also called the *gradient force*. The name *dipole force* comes from the fact that the force can be equivalently understood to arise from the polarisability of atoms in a light field, giving rise to a force identical to that which traps polarisable materials in optical tweezers [**?**].

2.1.4 Polarisation gradient cooling

Polarisation gradient cooling, also called Sisyphus cooling, was proposed in 1989 [**?**, 1] to explain experimentally measured cold atom cloud temperatures [**?**] which, at NIST in 1988, were found to be well below the expected limit obtainable by the well understood method of Doppler cooling[3], one of the few examples of experiments turning out better than expected. A one dimensional theory has been developed [1] which has found remarkable agreement with three dimensional experiments [**?**]

[3] As well as to explain other discrepancies between experiments and the theory of Doppler cooling, such as the optimal detuning of light being much greater than predicted.

One common configuration for Sisyphus cooling comprises two counterpropagating laser beams in each spatial dimension, both linearly polarised but with their polarisation angles perpendicular to one another. The optical field resulting from the two beams' superposition has regions of linear polarisation and of both helicities of circular polarisation, and varies between them on a length scale shorter than an optical wavelength.

The effect on multi-level atoms as they move from regions of one circular polarisation to another is that they are pumped alternately from one extreme of their spin-projection states to the other, alternately climbing and descending potential hills due to the dipole forces from the regions of different polarisations[4]. And so, like the Greek legend of Sisyphus[5], who was doomed to push a rock uphill for eternity, the atoms are climbing hills repeatedly. Due to the state dependence of the strength of the dipole forces, the atoms climb steeper hills than they descend, and are thus slowed and cooled.

[4] If you consider only one polarisation of light, its intensity varies sinusoidally in space, creating a series of potential hills and wells via the dipole force

This type of cooling does not work in a magnetic field; the splitting of transition frequencies makes it impossible for an atom to traverse its spin manifold on one laser frequency. For this reason the Sisyphus cooling stage is performed with magnetic fields off, though a sufficiently short period is required such that the atoms can be recaptured when the trapping field is restored.

[5] Polarisation gradient cooling is but one of a family of so called 'Sisyphus cooling' methods, all of which involve atoms repeatedly climbing potential hills.

2.1.5 Evaporative cooling

The final stage of cooling is forced RF evaporative cooling [**?**, **?**], which decreases the temperature of the cloud by systematically removing the hottest atoms. This is performed in a magnetic trap, which as mentioned earlier, only traps certain spin states. Evaporation proceeds by using an *RF knife* to induce spin flips in the atoms. The RF frequency is chosen such that is is only resonant with atoms some distance away from the center of the trap (via the Zeeman shift). The furthest out atoms are the most energetic, possessing the energy to climb the magnetic potential the furthest. By flipping their spins, these atoms are ejected due to the magnetic field becoming anti-trapping for them.

[6] So called because it cuts the tail off the velocity distribution of the atom cloud.

The cloud is given some time to rethermalise and the knife[6] is moved inward where it removes slightly colder atoms. This is repeated until the desired compromise of lower temperature/lower atom number is reached. Usually some method is employed to prevent atoms near the center of the trap from undergoing spin flips [**?**] as they move across the field zero. The method we'll employ is to use an optical dipole trap in combination with the magnetic trap [**?**], such that the coldest atoms get trapped in the dipole trap which is offset from the magnetic field zero.

```
rev:     84 (cf53f98d7d0e)
author:  Chris Billington
date:    Wed Oct 11 18:15:11 2017 -0400
summary: Working on atomic physics spin stuff
```

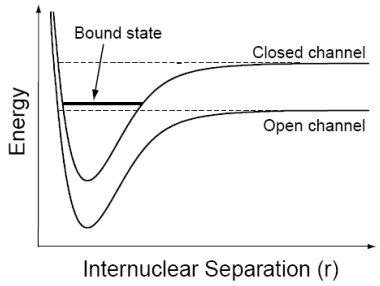

Figure 2.1: When atoms approach each other with spins aligned, they are in the *open channel*. In this channel they are unbound, but do not have enough energy to be free in the other channel - the *closed channel*. In the close range however, the atoms may have energy corresponding to a bound (molecular) state of the closed channel, a resonance which causes a divergence in the scattering length. The energy difference between the two channels can be tuned with a magnetic field and so these resonances can be induced in a wide range of situations.

2.1.6 Feshbach resonances

A Feshbach resonance [?] is an enhancement of the interparticle interaction strength when when a certain magnetic field strength is applied[7]. This phenomenon was first discovered in ultracold atoms in 1998 [?], and is now a staple of cold atom experiments.

[7] Feshbach resonances can also be induced optically and with RF but magnetic resonances are the most commonly used.

The interparticle interaction mentioned above:

$$g = \frac{2\pi\hbar^2 a}{m_r} \tag{2.5}$$

where m_r is the reduced mass of a pair of the interacting particles, is dependent on a parameter a called the *s-wave scattering length*, which characterises low energy collisions between atoms. It is sensitive not only to what species of atoms are colliding, but also to their spin states. For each combination of spins, there is a different inter-atomic potential (called a *channel*) which determines the collision dynamics (Figure 2.1).

The resulting scattering length is sensitive to any bound states of this inter-atomic potential which are near the collision energy. If the channels of different spin states are coupled via the hyperfine interaction[8], then the scattering length is also sensitive to bound states in the channels other the one the atoms are in when they are far from each other. Due to the Zeeman effect, the energies between the different channels can be shifted with a magnetic field, and so a bound state can be shifted close to the collision energy, which causes the scattering length to diverge.

[8] Requiring that the atoms in question have a nuclear magnetic moment.

The end result is that at certain magnetic field strengths we find that atoms are much more strongly attracted to or repelled from each other.

We plan to use a Feshbach resonance (Figure 2.2) to enhance the interspecies repulsion between ^{87}Rb and ^{41}K, thus trapping tracer particles more strongly in vortex cores.

2.2 Mean field theory: The Gross–Pitaevskii equation and vortices

Bose-condensates are described well by *mean field* theory, whereby the many-body wavefunction is approximated by a product of identical single-particle wavefunctions. Indeed, that the majority of the atoms are in the same quantum state is one of the defining features of BEC. The effect of interparticle interactions is included as a nonlinear term in the

```
rev:     84 (cf53f98d7d0e)
author:  Chris Billington
date:    Wed Oct 11 18:15:11 2017 -0400
summary: Working on atomic physics spin stuff
```

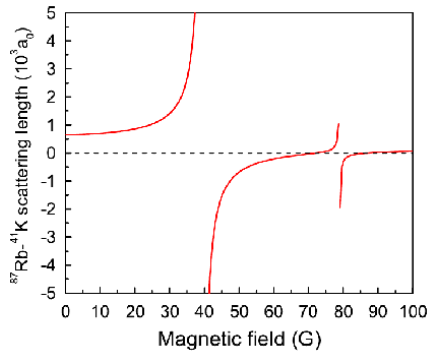

Figure 2.2: Predicted interspecies scattering length [?] as a function of magnetic field strength, for ^{41}K and ^{87}Rb both in their lowest energy hyperfine groundstate. The 35 gauss resonance is one of the main reasons for this pair of atoms being used in this project. It has a particularly low field strength and large width compared to most Feshbach resonances.

Schrödinger equation for the single particle wavefunctions, known as the Gross-Pitaevskii equation:

$$\frac{\partial \Psi}{\partial t} = \left[-\frac{\hbar^2}{2m}\nabla^2 + V(\boldsymbol{x}) + g|\Psi|^2 \right]\Psi, \tag{2.6}$$

where g characterises the strength of the interparticle interactions[9], and $\Psi = \sqrt{N}\Psi_{\text{single}}$ is the single-particle wavefunction scaled by the square root of the number of particles[10].

In the hydrodynamic formulation of quantum mechanics [?], the flow velocity of a spatial wavefunction can be defined by considering the probability current to be a product of density and velocity. This allows us to define the superfluid velocity of a BEC as:

$$\boldsymbol{v} = \frac{\hbar}{m}\nabla\phi \tag{2.7}$$

where ϕ is the phase of the condensate wavefunction Ψ. Integrating this velocity over any closed path γ gives us the circulation:

$$C = \frac{\hbar}{m}\oint_\gamma \nabla\phi \, ds \tag{2.8}$$

$$= \frac{\hbar}{m} 2\pi n. \qquad n = 0, 1, 2 \ldots \tag{2.9}$$

The fact that the circulation is quantised means that vorticity cannot exist in the condensate except in one-dimensional lines, about which the wavefunction's phase winds by a multiple of 2π. These topological defects are the quantised vortices that are central to this project.

At a vortex core, the atom density of a BEC must go to zero. This can be intuitively understood to arise from centrifugal forces, but is also required in order for the wavefunction to be continuous and single-valued across the core. This drop in density in the vicinity of a vortex core is what our method exploits in order to trap atoms within the cores.

[9] And is usually positive—having the effect of stabilising BECs by self-repulsion.

[10] Thus giving it the property that $|\Psi|^2$ is the particle density.

```
rev:     84 (cf53f98d7d0e)
author:  Chris Billington
date:    Wed Oct 11 18:15:11 2017 -0400
summary: Working on atomic physics spin stuff
```

2.3 Optical transitions on the ^{87}Rb D line

We atomic physicists do our theory work at an intermediate level of abstraction, at which many quantities and systems of interest can be computed and simulated with accurate models using standard quantum mechanics, but with the models not being fully a-priori. Instead, the Hamiltonians we feed to the machinery of standard quantum mechanics encapsulate some of the details we are not interested in or that are too hard to compute, with the link between the underlying layers of reductionism and the higher layer usually provided by experimentally measured constants rather than calculations from fundamental physics. In this way we can readily compute results about the atoms we are interested in by treating them as simpler systems than they actually are, with some of the the underlying details encapsulated by terms in an effective Hamiltonian for the dynamics that we are interested in.

In this section I'll summarise what the ^{87}Rb D line looks like from the perspective of a cold atom physicist, building up a Hamiltonian containing all 32 sublevels of the ground and first excited state of ^{87}Rb including fine structure, hyperfine structure, interaction with a magnetic field, and optical transitions between states. This Hamiltonian is the starting point for any calculations regarding cooling, trapping, and coherent control of ^{87}Rb, and the process for other alkali earth metals is much the same.

2.3.1 Fine structure

The rubidium 87 D line is not just one transition between a ground state and an excited state—there are two excited states, and the two resulting transitions are called, in order of their transition frequencies, the D_1 and D_2 lines. Thus the ground and first excited state of ^{87}Rb are actually a ground state plus two non-degenerate excited states, once we take into account fine structure. The groundstate is an S state (electronic orbital angular momentum quantum number $L = 0$), called the $S_{\frac{1}{2}}$ state, and the two excited states are P states ($L = 1$), one with the electron spin anti-aligned with its orbital angular momentum ($J = 1/2$) and one with the electron spin aligned with its orbital angular momentum ($J = 3/2$), called the $P_{\frac{1}{2}}$ and $P_{\frac{3}{2}}$ states respectively. In all of these states, ^{87}Rb's single outer-shell electron occupies an orbital with principle quantum number $n = 5$, which for brevity we leave out of the notation. The transition between $S_{\frac{1}{2}}$ and $P_{\frac{1}{2}}$ is called the D_1 line, with experimentally measured (angular) transition frequency ω_{D_1}, and the transition between $S_{\frac{1}{2}}$ and $P_{\frac{3}{2}}$ is the D_2 line with angular transition frequency ω_{D_2}. These transition frequencies correspond to optical wavelengths of $\lambda_{D_1} \approx 795$ nm and $\lambda_{D_2} \approx 780$ nm [2].

This fine structure is treated entirely empirically for our purposes, and so our base Hamiltonian for the rubidium D line, taking into account only fine structure, is simply a statement of the experimentally measured energy differences between the states:

[TODO: rename H_{fs} or $H_{D\,\text{fs}}$ or something]

$$\hat{H}_0 = \hat{0}_{S_{1/2}} \oplus \hbar\omega_{D_1} \hat{1}_{P_{1/2}} \oplus \hbar\omega_{D_2} \hat{1}_{P_{3/2}}, \tag{2.10}$$

where $\hat{0}_{S_{1/2}}$, $\hat{1}_{P_{1/2}}$, and $\hat{1}_{P_{3/2}}$ are zero and identity operators each acting on the subspace of states within the $S_{\frac{1}{2}}$, $P_{\frac{1}{2}}$, or $P_{\frac{3}{2}}$ manifold, and $\oplus$ is the direct sum.[11] The matrix representation H_0 of $\hat{H}_0$ in the basis in which it is diagonal is

$$H_0 = \begin{bmatrix} \begin{bmatrix} \ddots & & \\ & 0 & \\ & & \ddots \end{bmatrix} & & \\ & \begin{bmatrix} \ddots & & \\ & \hbar\omega_{D_1} & \\ & & \ddots \end{bmatrix} & \\ & & \begin{bmatrix} \ddots & & \\ & \hbar\omega_{D_2} & \\ & & \ddots \end{bmatrix} \end{bmatrix}, \tag{2.11}$$

[11] Not to be confused with the Kronecker sum, with which it shares notation. The direct sum concatenates matrices as blocks, producing a larger, block-diagonal matrix with dimension equal to the *sum* of the dimensions of the matrices being direct-summed, whereas the Kronecker sum is the the regular sum of matrices after each has been multiplied using the Kronecker-product with identity matrices with sizes of the other matrices in the sum, producing matrices with dimension equal to the *product* of those being summed.

```
rev:     84 (cf53f98d7d0e)
author:  Chris Billington
date:    Wed Oct 11 18:15:11 2017 -0400
summary: Working on atomic physics spin stuff
```

which is a block-diagonal matrix with each block also being a diagonal matrix. We have not yet specified the size of each submatrix—the size of each differs and depends on how many hyperfine and Zeeman sublevels are in that state.

This base Hamiltonian is worth pointing out since the energy differences between its three states are orders of magnitude larger than any of the energy differences between hyperfine and Zeeman sublevels within them. When doing any sort of calculations or simulations then, this time-independent Hamiltonian can be removed from the equations using an interaction picture, which we will come to shortly when we discuss optical transitions.

2.3.2 Hyperfine structure

Within each of the $S_{1/2}$, $P_{1/2}$ and $P_{3/2}$ states, the single outer-shell electron's total angular momentum $\hat{\boldsymbol{J}}$ has an interaction with ^{87}Rb's nuclear angular momentum $\hat{\boldsymbol{I}}$. This results in multiple discrete energy levels depending on the relative orientation of the two separate angular momenta. The interaction Hamiltonian for this hyperfine structure is [cite steck and the two references steck cites][12]:

$$\hat{H}_{\text{hfs}} = \frac{A_{\text{hfs}}}{\hbar^2}\hat{\boldsymbol{I}}\cdot\hat{\boldsymbol{J}} + \frac{B_{\text{hfs}}}{\hbar^2}\frac{3(\hat{\boldsymbol{I}}\cdot\hat{\boldsymbol{J}})^2 + \frac{3}{2}\hat{\boldsymbol{I}}\cdot\hat{\boldsymbol{J}} - I(I+1)J(J+1)}{2I(2I-1)J(2J-1)}, \tag{2.12}$$

where J is the total angular momentum quantum number of the electron, equal to either $\frac{1}{2}$ or $\frac{3}{2}$ depending on which state in the D line we are considering, $I = \frac{3}{2}$ is the total angular momentum quantum number of the nucleus, and A_{hfs} and B_{hfs} are empirically determined coupling constants. Here we see the boundary between the quantities we can calculate with the machinery of quantum mechanics and those that we cannot and need to determine empirically—this expression applies so long as J and I are good quantum numbers,[13] and the two terms are the dipolar and quadrupolar interactions [cite the review article] between two angular momenta, with the coupling constants determined empirically and encapsulating many details that are difficult to compute a-priori, such as relativistic effects and the exact shape of the electron orbitals given the presence of inner shell electrons. For the spherically-symmetric $S_{1/2}$ groundstate, there is no quadrupolar interaction and so B_{hfs} is only nonzero for the two P excited states.[14] The values of A_{hfs} and Bhfs for each of the three states of the D line can be found in [steck].

For a given state of the D line, we can construct the matrix representation H_{hfs} of $\hat{H}_{\text{hfs}}$ in the basis in which the z vector components $\hat{I}_z$ and $\hat{J}_z$ of $\hat{\boldsymbol{I}}$ and $\hat{\boldsymbol{J}}$ are diagonal by constructing matrix representations $\boldsymbol{I}_{\mathcal{I}\times\mathcal{J}}$ and $\boldsymbol{J}_{\mathcal{I}\times\mathcal{J}}$ of the operators $\hat{\boldsymbol{I}}$ and $\hat{\boldsymbol{J}}$ in that basis and then applying the expression (2.12). The subscript $\mathcal{I}\times\mathcal{J}$ on each of the matrices indicates that the matrix is a representation of its respective operator in the product space of the spaces $\mathcal{I}$ and $\mathcal{J}$ of the two individual nuclear and electronic angular momentum degrees of freedom.

To construct matrix representations of angular momentum operators in the product space $\mathcal{I}\times\mathcal{J}$, we first need their matrix representations $\boldsymbol{I}_{\mathcal{I}}$ and $\boldsymbol{J}_{\mathcal{J}}$ in their respective subspaces, which we will write as $\boldsymbol{I}$ and $\boldsymbol{J}$ for brevity. We can then expand the two operators into the total space by applying a Kronecker product with an appropriate identity matrix to each:

$$\boldsymbol{I}_{\mathcal{I}\times\mathcal{J}} = \boldsymbol{I}\otimes\mathbb{I}_{\mathcal{J}} \tag{2.13}$$

$$\boldsymbol{J}_{\mathcal{I}\times\mathcal{J}} = \mathbb{I}_{\mathcal{I}}\otimes\boldsymbol{J} \tag{2.14}$$

where $\mathbb{I}_{\mathcal{I}}$ is the matrix representation of the identity operator on the $\mathcal{I}$ subspace, equal to a $(2I+1)\times(2I+1)$ identity matrix, with $\mathbb{I}_{\mathcal{J}}$ defined similarly. Each of the two matrices is actually a vector of matrices, one for the angular momentum projection in each of

[12] Note that this expression differs from those in the cited references by a factor of $1/\hbar^2$—this is because I define the $\hat{\boldsymbol{I}}$ and $\hat{\boldsymbol{J}}$ angular momentum operators in SI units, rather than in units of $\hbar^2$.

[13] J is a good quantum number so long as the hyperfine splitting is small compared to the spacing between the three states of the D line, which it is, and I is a good quantum number so long as the hyperfine splitting is small compared to the energy difference between the groundstate and the first *nuclear* excited state, which it most certainly is.

[14] The quadrupolar term should be explicitly excluded from numerical computations of the hyperfine splitting on the $S_{1/2}$ state, as it contains a division by zero in this case, which may lead to erroneous results even if the term is subsequently multiplied by $B_{\text{hfs}} = 0$.

rev: 84 (cf53f98d7d0e)
author: Chris Billington
date: Wed Oct 11 18:15:11 2017 -0400
summary: Working on atomic physics spin stuff

the directions x, y and z. The procedure for constructing such matrices for arbitrary total angular momentum quantum numbers is as follows.[15] I'll show the procedure for constructing J_x, J_y and J_z only for an arbitrary J, the procedure is identical for computing the vector components of $\boldsymbol{I}$.

For a given total angular momentum quantum number J, the vector components of $\boldsymbol{J}$ in the z basis (the basis in which J_z is diagonal) can be constructed using the raising and lowering operators $\hat{J}_+$ and $\hat{J}_-$. Since the action of the raising and lowering operators on an eigenstate of J_z with angular momentum projection quantum number m_J is to produce an adjacent $(m_J \pm 1)$ eigenstate multiplied by a known constant [CITE SOME TEXTBOOK], this fact can be used to compute the nonzero matrix elements of $\hat{J}_+$ and $\hat{J}_-$ in the $\{|m_J\rangle\}$ basis:

$$\langle m_J|\hat{J}_+|m_J+1\rangle = \hbar\sqrt{J(J+1)-m_J(m_J+1)}, \qquad m_J < J, \tag{2.15}$$

$$\langle m_J|\hat{J}_-|m_J-1\rangle = \hbar\sqrt{J(J+1)-m_J(m_J-1)}, \qquad m_J > -J, \tag{2.16}$$

$$\tag{2.17}$$

and therefore compute explicit matrices for J_+ and J_- in the $\{|m_J\rangle\}$ basis:[16]

$$J_+ = \begin{bmatrix} 0 & \dots & & & & \\ \langle J-1|\hat{J}_+|J\rangle & 0 & \dots & & & \\ 0 & \langle J-2|\hat{J}_+|J-1\rangle & 0 & \dots & & \\ \dots & 0 & \langle J-3|\hat{J}_+|J-2\rangle & 0 & \dots & \\ & & \ddots & \ddots & \ddots & \\ & & \dots & 0 & \langle -J|\hat{J}_+|-J+1\rangle & 0 \end{bmatrix}, \tag{2.18}$$

$$J_- = \begin{bmatrix} 0 & \langle J|\hat{J}_-|J-1\rangle & 0 & \dots & & \\ \dots & 0 & \langle J-1|\hat{J}_-|J-2\rangle & 0 & \dots & \\ & & \ddots & \ddots & \ddots & \\ & & \dots & 0 & \langle -J+2|\hat{J}_-|-J+1\rangle & 0 \\ & & & \dots & 0 & \langle -J+1|\hat{J}_-|-J\rangle \\ & & & & \dots & 0 \end{bmatrix}, \tag{2.19}$$

both of which have nonzero values along only one non-main diagonal adjacent to the main diagonal, and which form a Hermitian conjugate pair (or indeed, a transpose pair, since all elements are real). The matrix representations of $\hat{J}_x$ and $\hat{J}_y$ can then be computed by rearranging the defining expressions [CITE] for $\hat{J}_+$ and J_-;

$$\hat{J}_+ = \hat{J}_x + \mathrm{i}\hat{J}_y, \tag{2.20}$$

$$\hat{J}_- = \hat{J}_x - \mathrm{i}\hat{J}_y, \tag{2.21}$$

for $\hat{J}_x$ and $\hat{J}_y$, and then applying the result to our matrix representations of $\hat{J}_+$ and $\hat{J}_-$ to obtain matrix representations J_x and J_y of $\hat{J}_x$ and $\hat{J}_y$ in the $\{|m_J\rangle\}$ basis:

$$J_x = \frac{J_+ + J_-}{2}, \tag{2.22}$$

$$J_y = \frac{J_+ - J_-}{2\mathrm{i}}. \tag{2.23}$$

Finally, since $\{|m_J\rangle\}$ is the eigenbasis of J_z with eigenvalues $\{\hbar m_J\}$, the matrix representation of J_z is simply the diagonal matrix of eigenvalues:

$$J_z = \begin{bmatrix} \hbar J & & & \\ & \hbar(J-1) & & \\ & & \ddots & \\ & & & -\hbar J \end{bmatrix}. \tag{2.24}$$

We can also construct the matrix representation J^2 of the total (squared) angular momentum operator $\hat{J}^2$ as

$$J^2 = J_x^2 + J_y^2 + J_z^2, \tag{2.25}$$

[16] We're using the standard convention of ordering the eigenvectors $\{|m_J\rangle\}$ in descending order of m_J. This is at odds with the computer programming convention of looping over most indices in ascending order, and so care should be taken when constructing these matrices in a computer program.

```
rev:     84 (cf53f98d7d0e)
author:  Chris Billington
date:    Wed Oct 11 18:15:11 2017 -0400
summary: Working on atomic physics spin stuff
```

or equivalently

$$J^2 = J(J+1)\hbar^2 \mathbb{I}_J, \tag{2.26}$$

since every m_J state is an eigenstate of the J^2 operator with eigenvalue $J(J+1)\hbar^2$.

The above prescription can be used to produce matrix representations of angular momentum operators J_x, J_y, J_z and J^2 for any integer or half-integer total angular momentum quantum number J. The three components can be considered a vector of matrices, J for the vector angular momentum operator $\hat{J}$. Below is a Python function that computes these matrices as well as the corresponding eigenvectors:

```python
import numpy as np
hbar = 1.054571628e-34

def angular_momentum_operators(J):
    """Construct matrix representations of the angular momentum operators Jx,
    Jy, Jz and J2 in the eigenbasis of Jz for given total angular momentum
    quantum number J. Return them, as well as the number of angular momentum
    projection states, a list of angular momentum projection quantum numbers
    mJ, and a list of their corresponding eigenvectors, in the same order as
    the matrix elements (in descending order of mJ)."""
    n_mJ = int(round(2*J + 1))
    mJlist = np.linspace(J, -J, n_mJ)
    Jp = np.diag([hbar * np.sqrt(J*(J+1) - mJ*(mJ + 1)) for mJ in mJlist if mJ < J], -1)
    Jm = np.diag([hbar * np.sqrt(J*(J+1) - mJ*(mJ - 1)) for mJ in mJlist if mJ > -J], 1)
    Jx = (Jp + Jm) / 2
    Jy = (Jp - Jm) / 2j
    Jz = np.diag([hbar*mJ for mJ in mJlist])
    J2 = Jx**2 + Jy**2 + Jz**2
    basisvecs_mJ = [vec for vec in np.identity(n_mJ)]
    return Jx, Jy, Jz, J2, n_mJ, mJlist, basisvecs_mJ
```

Using the above prescription to construct a matrix representation of the $\hat{J}$ operator with $J = \frac{1}{2}$ for the $S_{1/2}$ and $P_{1/2}$ states, or $J = \frac{3}{2}$ for the $P_{3/2}$ state, and to construct a matrix representation of the $\hat{I}$ operator with $I = \frac{3}{2}$, we are close to being able to explicitly construct a matrix representation of the hyperfine interaction Hamiltonian for any state of the ^{87}Rb D line. The remaining step is to obtain the matrix representations of the two operators in the $\mathcal{I} \times \mathcal{J}$ product space using (2.13) and (2.14), and then we can apply (2.12) to our matrices to obtain the matrix representation H_{hfs} of $\hat{H}_{\text{hfs}}$ for a given J corresponding to one of the three states on the D line:

$$H_{\text{hfs}} = \frac{A_{\text{hfs}}}{\hbar^2} \boldsymbol{I}_{\mathcal{I}\times\mathcal{J}} \cdot \boldsymbol{J}_{\mathcal{I}\times\mathcal{J}} + \frac{B_{\text{hfs}}}{\hbar^2} \frac{3(\boldsymbol{I}_{\mathcal{I}\times\mathcal{J}} \cdot \boldsymbol{J}_{\mathcal{I}\times\mathcal{J}})^2 + \frac{3}{2}\boldsymbol{I}_{\mathcal{I}\times\mathcal{J}} \cdot \boldsymbol{J}_{\mathcal{I}\times\mathcal{J}} - I(I+1)J(J+1)}{2I(2I-1)J(2J-1)}, \tag{2.27}$$

where the products of vector components within the dot products are computed with ordinary matrix multiplication. Alternatively, one can use the matrices in their individual subspaces rather than their equivalents in the product space, so long as one interprets the dot products as "Kronecker dot products":

$$H_{\text{hfs}} = \frac{A_{\text{hfs}}}{\hbar^2} \boldsymbol{I} \overset{\otimes}{\cdot} \boldsymbol{J} + \frac{B_{\text{hfs}}}{\hbar^2} \frac{3(\boldsymbol{I} \overset{\otimes}{\cdot} \boldsymbol{J})^2 + \frac{3}{2}\boldsymbol{I} \overset{\otimes}{\cdot} \boldsymbol{J} - I(I+1)J(J+1)}{2I(2I-1)J(2J-1)}, \tag{2.28}$$

where $\overset{\otimes}{\cdot}$ is the Kronecker dot product:

$$\boldsymbol{I} \overset{\otimes}{\cdot} \boldsymbol{J} \equiv I_x \otimes J_x + I_y \otimes J_y + I_z \otimes J_z. \tag{2.29}$$

In the above way one can construct an explicit matrix representation H_{hfs} for the hyperfine interaction for a given state of the D line. But what basis is it in? Because the matrix representations $\boldsymbol{I}$ and $\boldsymbol{J}$ of the electron and nuclear angular momentum operators

```
rev:     84 (cf53f98d7d0e)
author:  Chris Billington
date:    Wed Oct 11 18:15:11 2017 -0400
summary: Working on atomic physics spin stuff
```

were constructed in the $\{|m_I\rangle\}$ and $\{|m_I\rangle\}$ bases of their respective subspaces $\mathcal{I}$ and $\mathcal{J}$, the matrices we have constructed in the product space $\mathcal{I} \times \mathcal{J}$ are in the basis $\{|m_I\rangle\} \times \{|m_I\rangle\}$—the direct product of the two sets of basis vectors for the separate subspaces, with elements:

$$\{|m_I\rangle\} \times \{|m_J\rangle\} = \left\{ |m_I, m_J\rangle \,\middle|\, |m_I\rangle \in \{|m_I\rangle\}, |m_J\rangle \in \{|m_J\rangle\} \right\}, \tag{2.30}$$

where $|m_I, m_J\rangle = |m_I\rangle \otimes |m_J\rangle$ and $\otimes$ is the direct product of vectors.[17]

[17] Although the symbol $\otimes$ is used for both the Kronecker product and the direct product (of vectors), the direct product applies to vectors/state vectors, and the Kronecker product to matrices/operators. The direct product also applies to basis sets/spaces, but with the symbol $\times$. I would prefer nomenclature refer to them all with the same name and symbol, especially since the result of a direct product applied to an N-element column vector and an M-element column vector is identical to that of applying a Kronecker product to an $N \times 1$ matrix and a $M \times 1$ matrix, but I'll stick to the standard nomenclature.

The vector representation $\boldsymbol{\psi}$ of a state vector $|\psi\rangle$ in this basis is:

$$\boldsymbol{\psi} = \begin{bmatrix} \langle m_I = I, m_J = J|\psi\rangle \\ \langle m_I = I, m_J = J-1|\psi\rangle \\ \vdots \\ \langle m_I = I, m_J = -J|\psi\rangle \\ \langle m_I = I-1, m_J = J|\psi\rangle \\ \langle m_I = I-1, m_J = J-1|\psi\rangle \\ \vdots \\ \vdots \\ \langle m_I = -I, m_J = -J|\psi\rangle \end{bmatrix}. \tag{2.31}$$

The hyperfine Hamiltonian is not diagonal in the $\{|m_I, m_J\rangle\}$ basis. But, it is diagonal in the $\{|F, m_F\rangle\}$ basis, defined as the simultaneous eigenbasis of the $\hat{F}^2$ and $\hat{F}_z$ operators, which are the total (squared) and z component of the total angular momentum operator $\hat{\boldsymbol{F}} = \hat{\boldsymbol{I}} + \hat{\boldsymbol{J}}$, the matrix forms F^2 and F_z of which in the $|m_I, m_J\rangle$ basis can be constructed from the matrix forms of the individual angular momentum operators:

$$\begin{aligned} \boldsymbol{F}_{\mathcal{I}\times\mathcal{J}} &= \boldsymbol{I}_{\mathcal{I}\times\mathcal{J}} + \boldsymbol{J}_{\mathcal{I}\times\mathcal{J}} \\ &= \boldsymbol{I} \otimes \mathbb{I}_{\mathcal{J}} + \mathbb{I}_{\mathcal{I}} \otimes \boldsymbol{J} && (2.32) \\ F_{z\,\mathcal{I}\times\mathcal{J}} &= I_{z\,\mathcal{I}\times\mathcal{J}} + J_{z\,\mathcal{I}\times\mathcal{J}} \\ &= I_z \otimes \mathbb{I}_{\mathcal{J}} + \mathbb{I}_i \otimes J_z && (2.33) \\ F^2_{\mathcal{I}\times\mathcal{J}} &= \boldsymbol{F}_{\mathcal{I}\times\mathcal{J}} \cdot \boldsymbol{F}_{\mathcal{I}\times\mathcal{J}} && (2.34) \end{aligned}$$

The $\{|F, m_F\rangle\}$ basis allows the eigenstates of the hyperfine interaction to be labelled with F and m_F quantum numbers. For a states of the ^{87}Rb D line with electron total angular momentum quantum number J, there are $1 + J + I - |(J - I)|$ hyperfine levels, with F quantum numbers running from $|J - I|$ to $J + I$. Within each hyperfine level there are $2F + 1$ degenerate states with different m_F quantum numbers ranging from $-F$ to F. This results in a total of 32 possible states for the rubidium D line, a schematic of which is shown in Figure 2.3.

2.3.3 Zeeman sublevels

The states differing only in their m_F quantum numbers—called Zeeman sublevels—are degenerate in energy with respect to the hyperfine Hamiltonian, but an external magnetic field lifts this degeneracy. The Zeeman effect [CITE] results in an energy shift proportional to the external magnetic field $\boldsymbol{B}$ and to a system's magnetic moment $\boldsymbol{\mu}$:

$$V = -\boldsymbol{\mu} \cdot \boldsymbol{B}. \tag{2.35}$$

Our atom is a composite particle, made of a nucleus with its own magnetic moment, an electron with its own spin, and a contribution from the orbital motion of the electron about the nucleus. Each magnetic moment is proportional to the angular momentum of the subsystem in question, with the proportionality constants, called Landé g-factors

```
rev:     84 (cf53f98d7d0e)
author:  Chris Billington
date:    Wed Oct 11 18:15:11 2017 -0400
summary: Working on atomic physics spin stuff
```

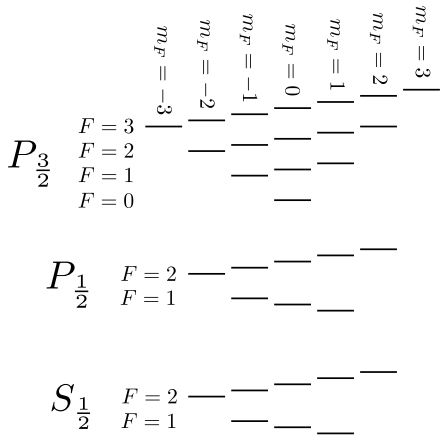

Figure 2.3: TODO: mention degeneracy of states and how F isn't a good quantum number

written as dimensionless multiples of $-\mu_B/\hbar$, where μ_B is the Bohr magneton.[18] Since J is a good quantum number so long as energy shifts are smaller than the (large) energy spacing between the three main states of the D line, on the level we work we don't consider the electron spin and orbital angular momenta separately, rather we roll them into one with a single, empirically determined Landé g-factor g_J for the magnetic moment of the electron in each of the three states. Similarly we consider the nucleus as a single spin with an experimentally determined g_I, resulting in a Zeeman Hamiltonian:

$$\begin{aligned}\hat{H}_Z &= -\hat{\boldsymbol{\mu}} \cdot \boldsymbol{B} && (2.36)\\ &= -\left(\hat{\boldsymbol{\mu}}_I + \hat{\boldsymbol{\mu}}_J\right) \cdot \boldsymbol{B} && (2.37)\\ &= \left(\frac{g_I \mu_B}{\hbar}\hat{\boldsymbol{I}} + \frac{g_J \mu_B}{\hbar}\hat{\boldsymbol{J}}\right) \cdot \boldsymbol{B}. && (2.38)\end{aligned}$$

Separate g_S and g_L values are known and can be used in two terms instead of the one containing $\hat{\boldsymbol{J}}$ above if J is not a good quantum number, but in the regime we work that is not usually the case (and if it were, the fine and hyperfine structure Hamiltonians above would also be inadequate). If J is a good quantum number then it is more accurate to use the above expression with empirically measured g_J values, since they encapsulate QED effects and corrections due to the multi-electron structure of ^{87}Rb that are not captured by the simple Zeeman Hamiltonian with separate $\hat{\boldsymbol{S}}$ and $\hat{\boldsymbol{L}}$ terms.

If the energy shift from the Zeeman effect is small compared to the hyperfine spitting, then F is a good quantum number and a given hyperfine level can be treated as a single magnetic moment subject to the Zeeman Hamiltonian:

$$\hat{H}_{Z\,\mathrm{lin}} = \frac{g_F \mu_B}{\hbar}\hat{\boldsymbol{F}} \cdot \boldsymbol{B}, \qquad (2.39)$$

where [cite steck]

$$g_F = g_J \frac{F(F+1) - I(I+1) + J(J+1)}{2F(F+1)} + g_I \frac{F(F+1) + I(I+1) - J(J+1)}{2F(F+1)}. \qquad (2.40)$$

The direction in which each Zeeman sublevel shifts in energy for small magnetic fields is depicted in Figure 2.3. Experimentally, Zeeman shifts that depart from this linear regime are often encountered, and so it is an approximation that cannot always be made.

```
rev:     84 (cf53f98d7d0e)
author:  Chris Billington
date:    Wed Oct 11 18:15:11 2017 -0400
summary: Working on atomic physics spin stuff
```

An explicit matrix representation H_Z of $\hat{H}_Z$ in the $\{|m_I, m_J\rangle\}$ basis for each of the three sates of the D line can be constructed by applying (2.38) to the matrix representations of $\hat{\boldsymbol{I}}$ and $\hat{\boldsymbol{J}}$ in that basis:

$$H_{Z\,\mathcal{I}\times\mathcal{J}} = -\boldsymbol{\mu}_{\mathcal{I}\times\mathcal{J}} \cdot \boldsymbol{B}, \tag{2.41}$$

where

$$\boldsymbol{\mu}_{\mathcal{I}\times\mathcal{J}} = -\frac{g_I \mu_B}{\hbar} \boldsymbol{I}_{\mathcal{I}\times\mathcal{J}} - \frac{g_J \mu_B}{\hbar} \boldsymbol{J}_{\mathcal{I}\times\mathcal{J}} \tag{2.42}$$

$$= -\frac{g_I \mu_B}{\hbar} \boldsymbol{I} \otimes \mathbb{I}_{\mathcal{J}} - \frac{g_J \mu_B}{\hbar} \mathbb{I}_{\mathcal{I}} \otimes \boldsymbol{J} \tag{2.43}$$

Here is a recap of what we have taken into account with our model of the Rubidium D line:

- The two lowest quantum numbers $L = 0$ and $L = 1$ of the electron's orbital angular momentum. This yields the S groundstate and P excited state.
- Fine structure: the two possible orientations of the electron's spin with respect to its orbital angular momentum. This splits the P excited state into two states, $P_{1/2}$ and $P_{3/2}$, and leaves the S groundstate as the single state $S_{1/2}$. The energies of these three states are determined entirely empirically—without any modelling of the fine structure.
- Hyperfine structure: The possible orientations of the electron's total angular momentum with respect to the nuclear angular momentum. This splits each state so far into $1 + J + I - |(J - I)|$ hyperfine states. The hyperfine interaction is treated semi-empirically, using an analytic form of the hyperfine interaction but with empirically determined coupling constants within each of the three states of the D line.
- Zeeman effect: the possible orientation of the total spin $\hat{\boldsymbol{F}}$ onto an external magnetic field. The Zeeman Hamiltonian is modelled analytically, but with empirically determined Landé g factors for each of the three states of the D line.

```
rev:     84 (cf53f98d7d0e)
author:  Chris Billington
date:    Wed Oct 11 18:15:11 2017 -0400
summary: Working on atomic physics spin stuff
```

References

[1] J. Dalibard and C. Cohen-Tannoudji. *Laser cooling below the Doppler limit by polarization gradients: simple theoretical models*. JOSA B **6**, 2023 (1989). DOI: 10.1364/JOSAB.6.002023. [p 7]

[2] D. A. Steck. Rubidium 87 D Line Data. steck.us/alkalidata, (2010). (revision 2.1.4). [p 10]

```
rev:     84 (cf53f98d7d0e)
author:  Chris Billington
date:    Wed Oct 11 18:15:11 2017 -0400
summary: Working on atomic physics spin stuff
```

This page intentionally left blank

Word count

```
Total
Words in text: 32393
Words in headers: 282
Words outside text (captions, etc.): 4690
Number of headers: 64
Number of floats/tables/figures: 31
Number of math inlines: 1118
Number of math displayed: 166
Files: 9
Subcounts:
  text+headers+captions (#headers/#floats/#inlines/#displayed)
  4049+48+783 (13/3/265/31) File(s) total: atomic_physics.tex
  725+17+385 (4/4/7/0) File(s) total: experiment.tex
  50+0+0 (0/0/0/0) File(s) total: front_matter.tex
  1370+19+65 (3/2/39/13) File(s) total: hidden_variables.tex
  1595+3+104 (2/0/12/0) File(s) total: introduction.tex
  20562+152+2572 (30/15/716/118) File(s) total: numerics.tex
  4+6+0 (1/0/0/0) File(s) total: software.tex
  4002+24+781 (8/7/79/4) File(s) total: velocimetry.tex
  36+13+0 (3/0/0/0) File(s) total: wave_mixing.tex
```

```
rev:     84 (cf53f98d7d0e)
author:  Chris Billington
date:    Wed Oct 11 18:15:11 2017 -0400
summary: Working on atomic physics spin stuff
```